Ultrasonics Sonochemistry 95 (2023) 106388

Contents lists available at ScienceDirect

Ultrasonics Sonochemistry

journal homepage: www.elsevier.com/locate/ultson

Simultaneous hydrodynamic cavitation and glow plasma discharge for the degradation of metronidazole in drinking water

Thiago Castanho Pereira [a], Erico Marlon Moraes Flores [a,*], Anna V. Abramova [b], Federico Verdini [c], Emanuela Calcio Gaudino [c], Fabio Bucciol [c], Giancarlo Cravotto [c]

[a] Department of Chemistry, Federal University of Santa Maria, Santa Maria, Brazil
[b] Kurnakov Institute of General and Inorganic Chemistry of the Russian Academy of Sciences, Moscow, Russia
[c] Department of Drug Science and Technology, Turin University, Turin, Italy

ARTICLE INFO

Keywords:
Hydrodynamic cavitation
Glow plasma discharge
Pharmaceutical degradation
Cavitation bubbles
Degradation of antibiotic compounds
Water treatment

ABSTRACT

In this study, a novel hydrodynamic cavitation unit combined with a glow plasma discharge system (HC-GPD) was proposed for the degradation of pharmaceutical compounds in drinking water. Metronidazole (MNZ), a commonly used broad-spectrum antibiotic, was selected to demonstrate the potential of the proposed system. Cavitation bubbles generated by hydrodynamic cavitation (HC) can provide a pathway for charge conduction during glow plasma discharge (GPD). The synergistic effect between HC and GPD promotes the production of hydroxyl radicals, emission of UV light, and shock waves for MNZ degradation. Sonochemical dosimetry provided information on the enhanced formation of hydroxyl radicals during glow plasma discharge compared to hydrodynamic cavitation alone. Experimental results showed a MNZ degradation of 14% in 15 min for the HC alone (solution initially containing 300×10^{-6} mol L^{-1} MNZ). In experiments with the HC-GPD system, MNZ degradation of 90% in 15 min was detected. No significant differences were observed in MNZ degradation in acidic and alkaline solutions. MNZ degradation was also studied in the presence of inorganic anions. Experimental results showed that the system is suitable for the treatment of solutions with conductivity up to 1500×10^{-6} S cm^{-1}. The results of sonochemical dosimetry showed the formation of oxidant species of 0.15×10^{-3} mol H_2O_2 L^{-1} in the HC system after 15 min. For the HC-GPD system, the concentration of oxidant species after 15 min reached 13×10^{-3} mol H_2O_2 L^{-1}. Based on these results, the potential of combining HC and GPD systems for water treatment was demonstrated. The present work provided useful information on the synergistic effect between hydrodynamic cavitation and glow plasma discharge and their application for the degradation of antibiotics in drinking water.

1. Introduction

The increase in the world's population and the outcome of infectious diseases lead to an increasing demand for antibiotic agents for human health [1]. Excessive use of antibiotics associated with their improper disposal and inefficient wastewater treatment systems have caused the release of these compounds into the environment [2,3]. Metronidazole (MNZ) is a nitroimidazole compound widely used in human health as a broad-spectra antibiotic against bacteria and protozoa infections [4,5]. MNZ is also commonly used in animal farming to prevent infectious diseases in poultry and fish [5-7].

MNZ presents a high persistence in the aquatic environment as a result of its high solubility in water and low biodegradability [8,9]. Furthermore, MNZ is also photostable and hydrophilic (logP = −0.1) [10]. Those physicochemical properties lead to a high impact of MNZ in aquatic organisms [11]. The presence of MNZ in environmental compartments can also induce the formation of bacterial strains resistant to its pharmacological effects [3,11].

Several technologies have been applied for the degradation of MNZ in wastewater, such as bioelectrochemical processes [12], biological degradation [13,14], dielectric barrier discharge [15], electrochemical degradation [16,17], Fenton oxidation [18-20], photocatalysis [21-23], ozonation [24,25], and sonochemical methods [26-28]. Most of the conventional biological processes for antibiotics degradation present limitations due to the high concentrations and toxicity of the compounds or their subproducts [29,30]. Physicochemical treatments require high

* Corresponding author.
E-mail address: ericommf@gmail.com (E.M.M. Flores).

https://doi.org/10.1016/j.ultsonch.2023.106388
Received 27 January 2023; Received in revised form 17 March 2023; Accepted 26 March 2023
Available online 29 March 2023

utilization of reagents, mostly oxidants, to treat highly concentrated polluted wastewater [31].

Cavitation-based processes have emerged as an alternative to wastewater treatment [32,33]. Cavitation processes are defined by the formation, growth, and implosion of cavitation bubbles in a short time [34]. During the formation of cavitation bubbles, due to the high inside temperature (up to 4600 K), there is a formation of reactive oxygen species (ROS) from the sonolysis of water molecules [34-36]. The collapse of cavitation bubbles generates strong shock waves and high-shear stress (up to 1000 bar), releasing high amounts of energy to liquid media [34,37].

The most common cavitation methods are acoustic cavitation (AC) and hydrodynamic cavitation (HC). In AC, bubbles are formed due to variations of pressure when a sound wave with a frequency between 20 kHz and 1 MHz is irradiated in a liquid media [36,38].

In HC, bubbles are formed due to changes in the pressure of a fluid passing through a constriction [39]. When the fluid passes through a constriction, there is an increase in kinetic energy and a decrease in pressure. If the pressure of the liquids falls below the vapor pressure of the liquid at the operating temperature, cavities are formed. After the flow of the liquid through the constriction, as the liquid jet kinetic energy decreases, the liquid pressure recovers, causing the collapse of the cavitation bubbles [39-41].

HC units may have a different setup: orifice plates, Venturi tubes, nozzles, vortex-based devices, or rotor/stator reactors [39,40,42]. HC reactors present better characteristics for scale-up and lower energy consumption than acoustic cavitation-based reactors [43]. HC technology can also be combined with different advanced oxidation processes (AOPs) for process intensification in wastewater treatment [44].

Recently, some studies have shown the use of HC coupled to glow plasma discharge [45,46]. The combination of cavitation bubbles and highly reactive conditions during glow plasma discharge produces synergistic effects for organic pollutants degradation [45-47]. Due to the low electron mobility in the bulk solution, the charges from glow plasma discharge are conducted through the surface of cavitation bubbles [47,48]. Furthermore, due to the conduction of charges in the surface of cavitation bubbles with low internal pressure (i.e., low pressure at the flow through constriction), the internal gas content of the bubbles can be ionized [49-51]. This process induces the formation of highly reactive oxygen species, UV-light emission, and ozone formation, contributing to more robust organic pollutants degradation [45,46].

Therefore, the aim of the present work is to demonstrate the use of HC combined with glow plasma discharge for the degradation of metronidazole in drinking water. Experiments were carried out to demonstrate the applicability and robustness of the system for the degradation of pollutants in drinking water.

2. Methodology

2.1. Reagents

Metronidazole (98%), ammonium molybdate tetrahydrate (99.96%), hydrogen peroxide (34.5 to 36.5%), sodium chloride (99%), and sodium hydroxide (98%) were obtained from Sigma Aldrich. Potassium iodate (99%) was purchased from Alfa Aesar. Ethanol (99.8%) was provided by WVR Chemicals. Sulfuric acid was provided by Thermo Scientific. Sodium bicarbonate (98%) was purchased from Solvay. Deionized water (conductivity $< 2 \times 10^{-6}$ S cm^{-1}) was used to prepare the aqueous solutions.

2.2. Experimental procedure

Before each experiment, 10 L of a 300×10^{-3} mol L^{-1} MNZ solution was prepared with distilled water. Solution pH was measured before the experiments with a pHmeter (pH 211, Hanna Instruments, USA). The pH of a freshly prepared MNZ solution without any pH adjustment is 5.80. Therefore, for the experiments, initial pH of 5.80 was arbitrarily selected. For experiments in acidic (pH = 4.0) or alkaline (pH = 9.0), a 0.1 mol L^{-1} H_2SO_4 or a 0.1 mol L^{-1} NaOH solution were used, respectively. Solution conductivity was measured prior to degradation experiments with a conductivity meter (2510-A40103 Tec-4MP, Tecnal, Brazil). Degradation processes were carried out in a HC coupled to a glow plasma discharge (HC-GPD) reactor, shown in Fig. 1.

The discharge chamber consisted of a cylindrical quartz tube with a 40 cm height and 1.2 cm diameter. In the upper part of the reactor, an orifice plate was placed as a HC unit. The orifice plate consisted of a 2 cm diameter brass plate with four holes with a diameter of 0.4 cm each. The cavitation number (Cv) of the system can be calculated with Equation 1.

$$C_v = \frac{p_2 - p_v}{\frac{1}{2}(\rho v_0^2)} \quad (1)$$

where p_2 (Pa) is the downstream pressure, p_v is the vapor pressure of the liquid (Pa), v_0 is the fluid velocity at the cavitating device (m s^{-1}), and ρ is the density of the liquid (kg m^{-3}). In HC unit, the measured pressure downstream of the orifice plate was 16212 Pa (the manometric pressure in the downstream of cavitation emitter was measured with a manometer), and the fluid velocity at the cavitating device was 99 m s^{-1} (this value was calculated from the HC device model using COMSOL Multiphysics software). For water at 25 °C, the vapor pressure is 3160 Pa, and the density is 997.07 kg m^{-3}. Therefore, for HC system $C_v = 0.0027$.

For the glow plasma discharge, two electrodes made of brass with 5 cm height and 0.4 cm thickness were placed at a distance of 20 cm. The electrodes were connected to a continuum current power supply with a voltage of 15 kV and a current of 0.33 A. The power supply was equipped with an LCD screen that showed the applied power for plasma discharge. The overall power consumption of the system was 21.85 kWh.

For the experiments with plasma discharge, two modes were tested. In the pulsed glow plasma discharge (HC-PGPD), the pulses lasted for one minute of plasma on, followed by one minute with plasma off. For continuous glow plasma discharge (HC-GPD), the plasma was on until the finish of the treatment.

A hydraulic pump (NP10/10-150, Speck, Germany), equipped with a manometer, was utilized for the liquid circulation with a pressure of 70 bar, and flowrate of 5.5 L min^{-1}, with a fluid velocity of 1.82 m s^{-1}. The recirculating liquid was cooled down using a chiller system (Miles 350 W, Cooltech, Italy).

The degradation experiments were carried out for 15 min. For collecting each sample, ethanol (10% v/v) was used to quench any radical reactions before MNZ measurement [52].

2.3. Analytical methods

The MNZ concentration in the aqueous solution was determined using a UV–Vis spectrophotometer (Varian Cary 50, Agilent Technologies, USA). UV–Vis spectra were recorded using a 1 cm quartz cuvette, in the 200 to 800 nm range, with an MNZ maximum absorption peak at 320 nm ($\varepsilon = 9185$ mol L^{-1} cm^{-1}). The measurement of oxidant species formation was carried out with Weissler dosimetry, as described in the literature [53]. For this procedure, 1 mL of a 0.4 mol L^{-1} KI, 0.05 mol L^{-1} NaOH, and 1.6×10^{-4} mol L^{-1} $(NH_4)_6Mo_7O_{24}{\cdot}4H_2O$) solution was mixed with 1 mL of a 0.1 M $KHC_8H_4O_4$ solution, and 1 mL of treated solution. The formation of triiodide ions was measured with a UV–Vis spectrophotometer (Varian Cary 50, Agilent Technologies, USA) at a wavelength of 350 nm.

2.4. Kinetic modeling and statistical methods

The kinetics of MNZ degradation was assessed by fitting the experimental data to pseudo-first-order kinetic model. The pseudo-first-order kinetic model is described by Equation 2, which is a first-order differ-

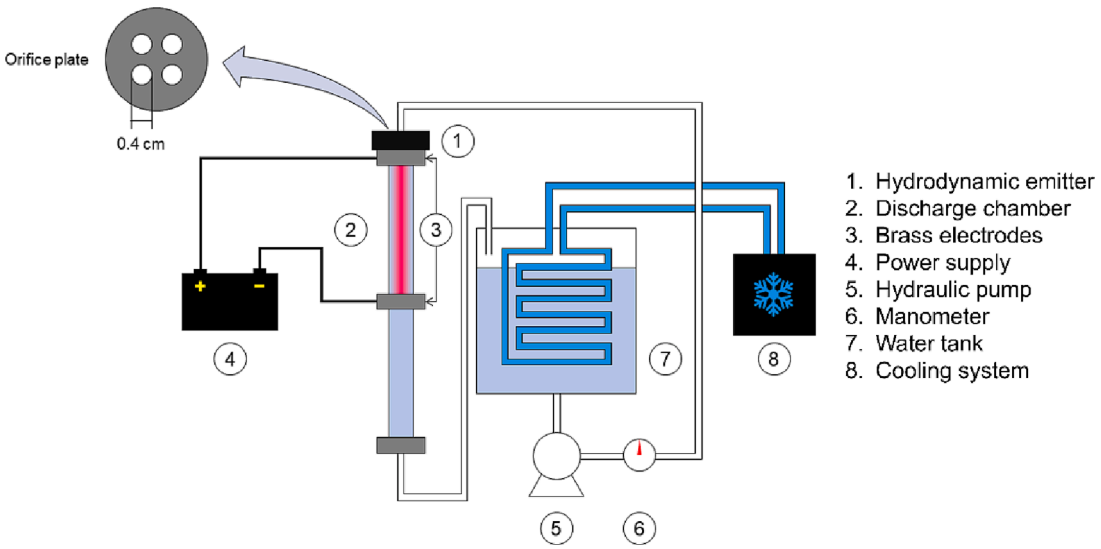

Fig. 1. Experimental setup of HC and plasma discharge reactor.

ential equation (ODE) whose analytical solution is given by Equation 3.

$$\frac{d[MNZ]}{dt} = -k \cdot [MNZ] \quad (2)$$

$$[MNZ] = [MNZ]_0 \cdot e^{-k \cdot t} \quad (3)$$

where *[MNZ]* is the concentration of MNZ in mol L^{-1} in the sample, $[MNZ]_0$ is the initial concentration of MNZ, and k is the reaction rate constant.

For kinetic modeling, k was tuned on MNZ experimental results as a function of time using the Levenberg-Marquardt method of optimization using Origin 2021 software.

In order to verify statistical significant differences between experiments, a *t*-test was used to compare the means of two groups, and ANOVA test was used to compare the means of more than two groups, utilizing GraphPad Instat software.

3. Results

3.1. Effect of the treatment process

To evaluate the effect of the degradation process and its impact on MNZ degradation, experiments were carried out in HC, HC with pulsed glow plasma discharge (HC-PGPD), and HC with continuous glow plasma discharge (HC-GPD). The results are shown in Fig. 2.

It was noticed a difference in MNZ degradation between all treatments ($p < 0.05$). Lower degradation rates were observed for the treatment using only HC compared to the degradation process coupled with plasma discharge. For HC-GPD treatment, a pseudo-first-order kinetic constant of 0.174 ± 0.006 min^{-1} was observed, 18 times higher than the pseudo-first-order kinetic constant observed for the HC process, 0.009 ± 0.001 min^{-1}. In HC processes, the main pathway for organic molecule degradation is the formation of •OH radicals formed in the collapse of cavitation bubbles [43,54].

Comparing the process using glow plasma discharge, HC-PGPD, and HC-GPD, it was possible to observe a higher degradation in the process with continuous discharge instead of the pulsed discharge mode. This result indicates the strong effect of plasma discharge on establishing synergistic effects in the degradation of MNZ. In the absence of cavitation bubbles, it was not observed any plasma discharge. Similar behavior was also observed for acoustic cavitation, with the coupling of an ultrasound probe with plasma discharge [47].

In glow plasma discharge, the electrical discharge in a liquid media

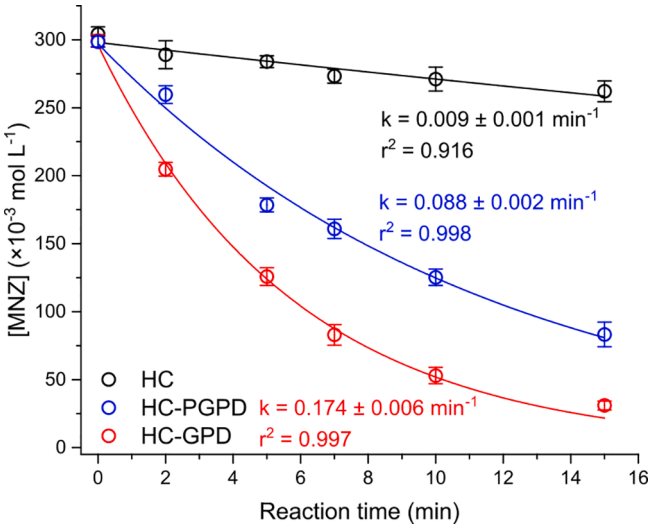

Fig. 2. Degradation of MNZ using HC reactor and pseudo-first order kinetic constants for degradation reactions. Dots represent experimental data and continuous line the pseudo-first-order kinetic model for MNZ degradation. Experimental conditions: $[MNZ]_0 = 300 \times 10^{-3}$ mol L^{-1}, Discharge voltage = 15 kV, Initial pH = 5.80, Inlet pressure = 70 bar, Number of orifices = 4, Orifice size = 4 mm, Initial temperature = 14 °C, Number of replicates = 2.

containing gas bubbles can induce the formation of hydroxyl radicals, hydrogen peroxide, atomic oxygen, ozone, and emission of UV light [55]. Hydroxyl radicals (•OH) are the major oxidant species in plasma discharge [55,56]. However, due to the short lifetime of •OH radicals (~3.7 × 10^{-9} s) and its short diffusion in bulk solution (~6 × 10^{-9} m) [55,57], most of the MNZ oxidation occurs in the interface of cavitation bubbles.

Previous works utilizing a similar HC-GPD system demonstrated a UV light emission at 300 nm [46]. Most of the research on MNZ photodegradation published in the literature uses UV-A lamps with a maximum UV light emission at 254 nm [58-60]. However, Shemer et al. observed MNZ degradation utilizing a medium-pressure mercury lamp with a UV-light emission range of 200 to 400 nm [61]. Due to the strong synergistic effects of cavitation bubbles and plasma discharge, it is challenging to estimate the contribution of each process (i.e. oxidation by •OH, photodegradation, and pyrolysis) to MNZ degradation in HC-

GPD treatment. Nevertheless, the above results demonstrate the advantages of coupling HC and glow plasma discharge for the degradation of MNZ in drinking water.

3.2. Effect of pH

The effect of solution pH was investigated in pH values of 4.0 and 9.0, which are generally the lower and higher pH observed in most wastewater discharges [62]. Freshly prepared MNZ solution presents a pH of 5.8, which was the pH chosen for optimization experiments. The effects of pH on MNZ degradation during HC-GPD treatment are shown in Fig. 3A. Comparing pH values of 4.0, 5.8, and 9.0, no statistical differences were observed in the pseudo-first-order kinetic constants (ANOVA, $p > 0.05$). For pH = 4.0 it was observed a kinetic constant of 0.141 ± 0.013 min^{-1}, with 88% of MNZ degradation in 15 min. For pH = 9.0, it was observed a kinetic constant of 0.142 ± 0.007 min^{-1}, with 88% of MNZ degradation in 15 min. MNZ molecule has a pKa = 2.58 [63]. Therefore, with a pH value higher than 2.58, the molecule presents charges in the nitrogen atom of the imidazole ring [63].

As shown in Fig. 3B, it was observed a pH decrease during MNZ degradation in HC-GPD. For all experiments, the final pH presented values of 3.0 to 3.3. pH decreases during organic pollutants degradation with plasma discharge are mainly due to carboxylic acids forming as a degradation product [56]. Furthermore, a reduction in the pH can contribute to organic pollutants degradation since the oxidative potential of $^{\bullet}$OH radical is higher in a pH near 3.0 ($E^0 = 2.70$ V) compared to an alkaline pH near 9.0 ($E^0 = 2.34$ V) [56].

3.3. Effect of the aqueous matrix

To verify the effects of aqueous matrix constituents in MNZ degradation with HC-GPD system, an experiment was conducted using potable water. The water utilized in this experiment was provided by SMAT (Società Metropolitana Acque Torino), the company responsible for potable water distribution in Turin, Italy. Results of MNZ degradation are shown in Fig. 4, and the physicochemical characterization of the drinking water is shown in Table 1.

According to Fig. 4, it is possible to observe a pseudo-first-order kinetic constant of 0.136 ± 0.002 min^{-1}, with 86% of MNZ degradation in 15 min. The results in drinking water are lower than observed for distilled water, 0.174 ± 0.06 min^{-1}, with 90% of MNZ degradation in 15 min. Considering the values of the hardness of drinking water, it can be regarded as very hard water [64]. Inorganic anions and organic substances like alcohols and solvents present in water can act as radical scavengers for $^{\bullet}$OH radicals.

The presence of scavengers causes a decrease in the degradation rate of MNZ since there is a competition between the radicals and MNZ to react with $^{\bullet}$OH radicals [56]. The reaction of carbonate and bicarbonate anions with $^{\bullet}$OH radicals promotes to the formation of carbonate radicals ($^{\bullet}CO_3^-$) according to Reactions 1 and 2, respectively [56].

$$CO_3^{2-} + {}^{\bullet}OH \rightarrow {}^{\bullet}CO_3^- + OH^- \quad (1)$$

$$HCO_3^{2-} + {}^{\bullet}OH \rightarrow {}^{\bullet}CO_3^- + H_2O \quad (2)$$

For Reaction 1, the pseudo-second-order kinetic constant is $k = 4.0 \times 10^8$ mol^{-1} s^{-1}, and for Reaction 2, the pseudo-second-order kinetic constant is $k = 1.0 \times 10^7$ mol^{-1} s^{-1} [65]. Therefore, considering the magnitude of reaction constants, the reaction of hydroxyl with carbonate and bicarbonate to form $^{\bullet}CO_3^-$ radicals is faster than the reaction with MNZ. Carbonate radicals have a lower oxidation potential ($E^0 = 1.63$ V) [65] than hydroxyl radicals ($E^0 = 2.34$ to 2.70 V). Therefore, the oxidation rate of organic compounds driven by $^{\bullet}CO_3^-$ radical attack is lower compared to $^{\bullet}$OH radicals [56]. As mentioned above, alcohols can also scavenge $^{\bullet}$OH radicals. The reaction of ethanol with hydroxyl radicals is described in Reaction 3.

$$CH_3CH_2OH + \cdot OH \rightarrow \cdot CH_2CH_2OH + H_2O \quad (3)$$

The pseudo-second-order kinetic constant for Reaction 3 is $k = 3.1 \pm 0.4 \times 10^{12}$ cm^{-1} mol^{-1} s^{-1} [66]. In the presence of ethanol in a concentration of 50×10^{-3} mol L^{-1}, it was observed a pseudo-first-order reaction constant of 0.0601 ± 0.002 min^{-1} for MNZ degradation, with 60% of MNZ degradation in 15 min of reaction. Those results corroborate the hypothesis of hydroxyl radical oxidation on MNZ degradation in HC-GPD processes.

The presence of inorganic constituents in aqueous solution can also influence the plasma discharge [47,50]. For the experiments with distilled water and tap water, the input voltage for plasma discharge was kept at 15 kV. However, for experiments with tap water was possible to observe instabilities in the discharge chamber. In Fig. 5 is possible to observe the delivered power for plasma discharge during experiments with distilled and tap water.

During plasma discharge in distilled water (conductivity $< 2 \times 10^{-6}$ S cm^{-1}), the delivered power showed a uniform behavior and reached values around 5 kW during plasma discharge. For experiments using tap water (conductivity $= 451 \times 10^{-6}$ S cm^{-1}), the initial delivered power was lower (around 3.34 kW) compared to distilled water. It

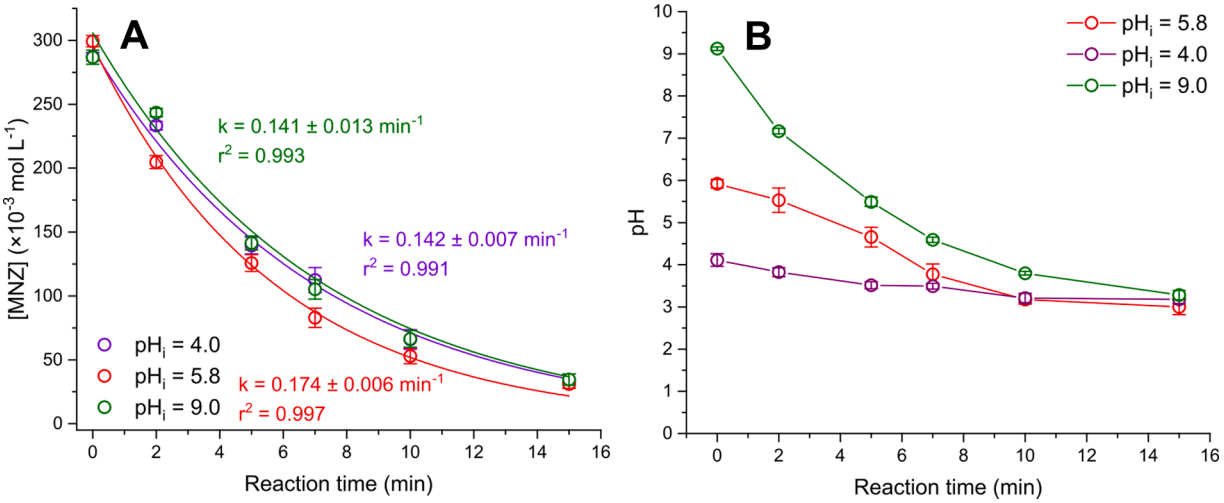

Fig. 3. (A) Effect of solution pH on the degradation of MNZ in the HC reactor and (B) variation of pH along the experiment. Dots represent experimental data and continuous line the pseudo-first-order kinetic model for MNZ degradation. Experimental conditions: $[MNZ]_0 = 300 \times 10^{-3}$ mol L^{-1}, Discharge voltage = 15 kV, Inlet pressure = 70 bar, Number of orifices = 4, Orifice size = 4 mm, Initial temperature = 14 °C, Number of replicates = 2.

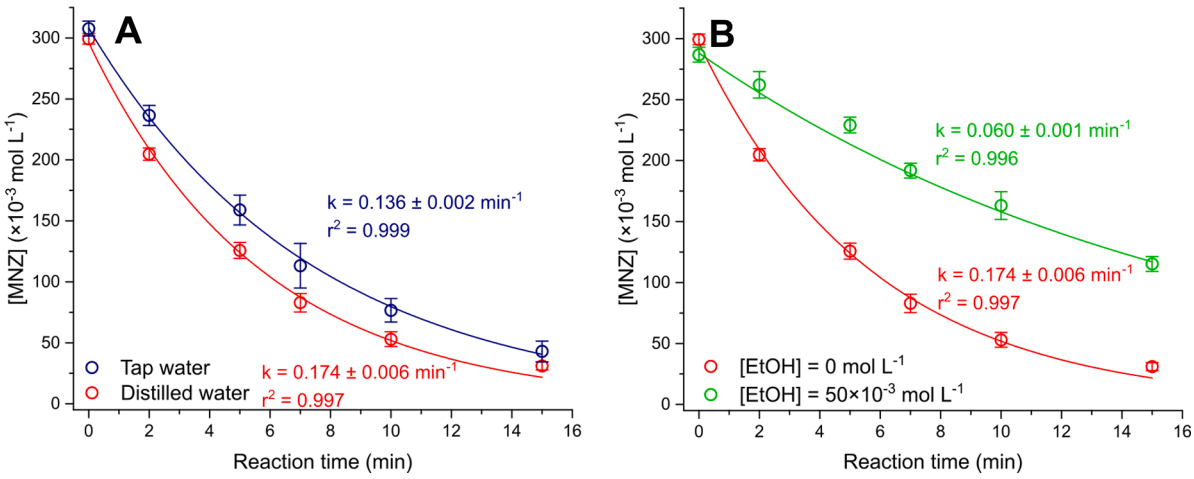

Fig. 4. Effect of (A) utilization of drinking water and distilled water and (B) scavenging effect of EtOH on the degradation of MNZ in the HC-GPD treatment. Dots represent experimental data and continuous line the pseudo-first-order kinetic model for MNZ degradation. Experimental conditions: $[MNZ]_0 = 300 \times 10^{-3}$ mol L^{-1}, Discharge voltage = 15 kV, Initial pH = 5.80, Inlet pressure = 70 bar, Number of orifices = 4, Orifice size = 4 mm, Initial temperature = 14 °C, Number of replicates = 2.

Table 1
Characteristics of the drinking water used in the experiments.

Parameter	Value
pH	7.50
Conductivity (μS cm^{-1})	451
Hardness (mg $CaCO_3$ L^{-1})	230
Chloride (mg L^{-1})	16
Sulfate (mg L^{-1})	36
Nitrate (mg L^{-1})	20
Bicarbonate (mg L^{-1})	228

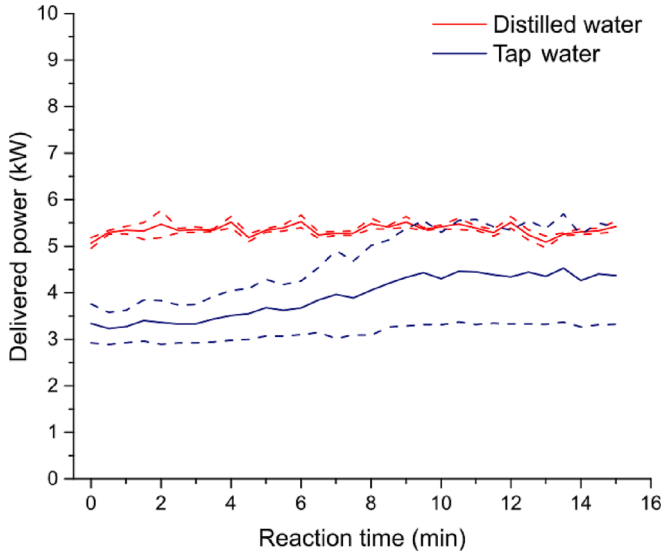

Fig. 5. Delivered power oscillations during plasma discharge in distilled and tap water solutions. Continuous line represents the average measurements, dashed line represents standard deviation. Experimental conditions: Discharge voltage = 15 kV, Inlet pressure = 70 bar, Number of orifices = 4, Orifice size = 4 mm, Initial temperature = 14 °C, Number of replicates = 4.

was also possible to observe a higher deviation of delivered power values from tap water than from distilled water. Changes in solution conductivity alter the charges conduction during plasma discharge [51]. An increase in conductivity causes a decrease in breakdown pulse duration and a reduction in the plasma channels. Therefore, due to the lower contact time and lower plasma interaction area in the interface of bubbles and bulk solution, the quenching of radicals formed during discharge is faster. This effect leads to the decrease of applied power during plasma discharge, due to shorter time [49,51].

Explaining the single effect of inorganic ions in solution in plasma discharge is difficult due to the strong synergistic effects. Changes in the chemical composition of the aqueous solution utilizing inorganic salts (e.g., NaCl and $NaHCO_3$) introduce a source of radical scavengers (i.e., Cl^- and HCO_3^-) and also lead to changes in conductivity.

To estimate the overall effect of dissolved salts on MNZ degradation in HC-GPD system, NaCl and $NaHCO_3$ were arbitrarily selected due to the ubiquitous presence of Cl^- and HCO_3^- anions in drinking water [67]. For those experiments, 300×10^{-3} mol L^{-1} MNZ solution were freshly prepared in distilled water. NaCl and $NaHCO_3$ were added separately, in two levels of concentration, in order to obtain solutions with different conductivities. Experimental results are shown in Fig. 6.

For experiments with bicarbonate anion (HCO_3^-), pseudo-first-order kinetic constants of 0.112 ± 0.003 min^{-1} and 0.112 ± 0.004 min^{-1} were observed for 2×10^{-3} mol l^{-1} and 4×10^{-3} mol l^{-1} HCO_3^- concentrations, respectively. Solution conductivity ranged from 896×10^{-6} S cm^{-1} for 2×10^{-3} mol l^{-1} HCO_3^- solution and 1812×10^{-6} S cm^{-1} for 4×10^{-3} mol l^{-1} HCO_3^- solution. Even with a 2-fold difference in solution conductivity, using a *t*-test, it was not observed a significant difference ($p > 0.05$) in kinetic constants between experiments.

In experiments with chloride anion (Cl^-), pseudo-first-order kinetic constants of 0.095 ± 0.008 min^{-1} and 0.099 ± 0.003 min^{-1} were observed for 0.45×10^{-3} mol l^{-1} and 2×10^{-3} mol l^{-1} HCO_3^- concentrations, respectively. Solution conductivity ranged from 349×10^{-6} S cm^{-1} for 0.45×10^{-3} mol $l^{-1}Cl^-$ solution and 1551×10^{-6} S cm^{-1} for 2×10^{-3} mol $l^{-1}Cl^-$ solution. With a 4.44-fold difference in solution conductivity, using a *t*-test, it was not observed a significant difference ($p > 0.05$) in kinetic constants between experiments.

Comparing the effects of experiments with HCO_3^- and Cl^- anions with distilled water, it is possible to observe pseudo-first-order kinetics 1.55 times lower for HCO_3^- experiments and 1.84 times lower for Cl^- experiments. The influence of separated anions in the plasma discharge process in aqueous solutions is not well described in the literature yet.

Fang et al. (2019) explored the effect of conductivity in plasma discharge in an acoustic cavitation plasma discharge assisted system, treating a reactive black 5 (RB5) dye solution. The authors observed

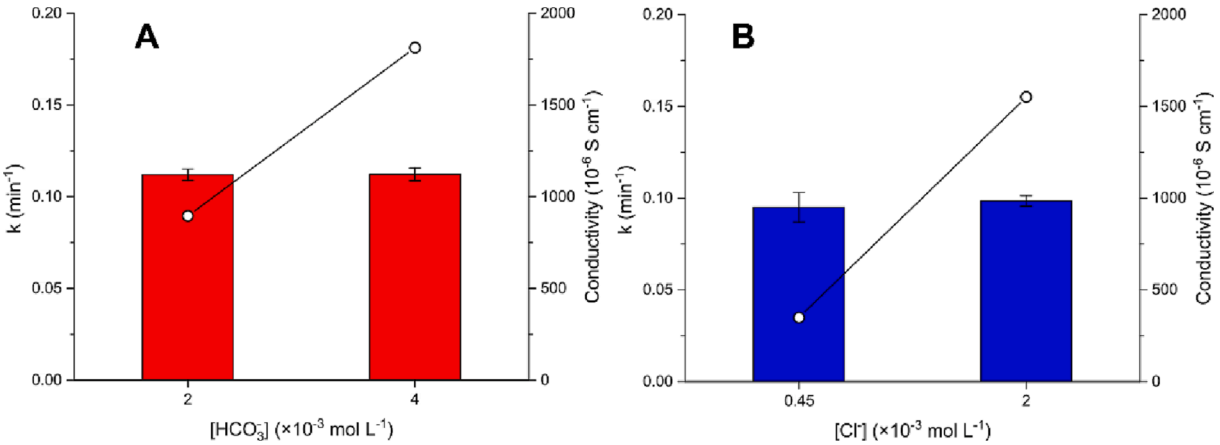

Fig. 6. Effect of (A) bicarbonate anion and (B) chloride anion on the degradation of MNZ in the HC-GPD system. Bars represent the pseudo-first-order kinetic constant, and scatter represent solution conductivity. Experimental conditions: $[MNZ]_0 = 300 \times 10^{-3}$ mol L^{-1}, Discharge voltage = 15 kV, Initial pH = 5.80, Inlet pressure = 70 bar, Number of orifices = 4, Orifice size = 4 mm, Initial temperature = 14 °C, Number of replicates = 2.

highest RB5 degradation in solutions with a conductivity ranging from 10 to 20 × 10^{-6} S cm^{-1} for a plasma discharge under US field. It was observed a decrease in RB5 degradation with the increase of solution conductivity. The conductivity upper limit for plasma discharge was observed at 1000 × 10^{-6} S cm^{-1} [47]. In a high conductivity solution, the breakdown process necessary for plasma discharge is hindered due to the ion flow, which induces a polarization in the electric field [50].

Therefore, detailed experiments must be carried out using chemical probes and measurement of radical species spectroscopic emission to understand the charges conduction in different chemical aqueous conditions [51].

Inorganic ions addition can also influence the behavior of cavitation bubbles. An increase in salt concentration causes a decrease in cavitation bubble size [68] and inhibits bubble coalescence [38]. Due to the salting-out effect, the presence of electrolytes also leads to a decrease in gas solubility in an aqueous solution, influencing the population of active bubbles. Furthermore, electrolytes also affect the surface tension and viscosity of the liquid, which can affect the cavitation bubble formation and its implosion [38].

However, considering the overall effect of the presence of inorganic constituents in tap water, according to the results presented in Fig. 4B, the degradation of MNZ in HC-GPD system is possible, presenting 86% degradation compared to 90% of degradation in distilled water, after 15 min of treatment.

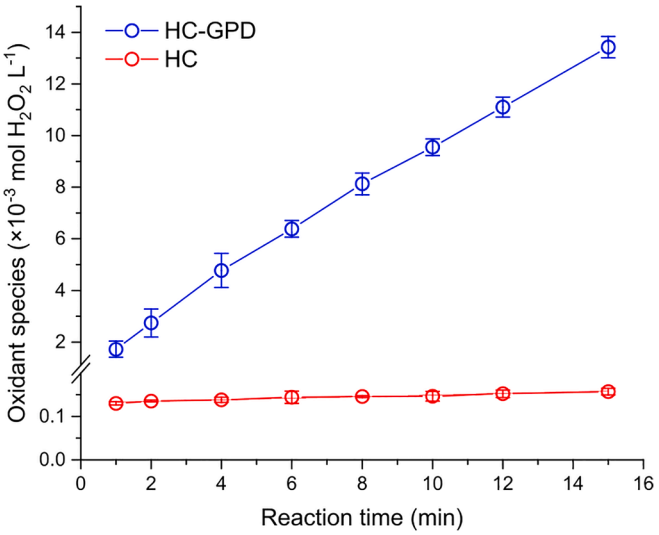

Fig. 7. Measurement of oxidant species formed during HC and HC-GPD process by Weissler dosimetry. Experimental conditions: Distilled water, Discharge voltage = 15 kV, Initial pH = 5.80, Inlet pressure = 70 bar, Number of orifices = 4, Orifice size = 4 mm, Initial temperature = 14 °C, Number of replicates = 2.

3.4. Sonochemical dosimetry

In order to estimate the formation of oxidant species during plasma discharge, Weissler dosimetry was carried out in experiments with only HC and HC coupled to glow plasma discharge (HC-GPD). The production of oxidant species is shown in Fig. 7.

Weissler dosimetry is based on the reaction of hydrogen peroxide formed during $^{\bullet}$OH produced with potassium iodide. I^- ions suffer oxidation by H_2O_2 and $^{\bullet}$OH to form I_2. The I_2 molecules formed react with the excess of I^- in solution to form a triiodide complex, which can be measured with a UV–Vis spectrophotometer at 353 nm. However, those oxidation reactions are not selective to H_2O_2 and $^{\bullet}$OH, other oxidant species formed can also influence the formation of the triiodide complex [38].

For experiments using HC alone, it was possible to observe a steady formation of oxidant species in the range of 0.12 to 0.15 × 10^{-3} mol H_2O_2 L^{-1} within 15 min of the process. For the HC-GPD process, it was observed a linear enhancement in the formation of oxidant species. Along reaction time was possible to observe a concentration of 13.4 ± 0.41 × 10^{-3} mol H_2O_2 L^{-1} after 15 min. Plasma discharge in aqueous solution increased 87 times the formation of oxidant species, in a formation rate of 0.898 ± 0.025 × 10^{-3} mol H_2O_2 L^{-1} min^{-1} (r^2 = 0.994). Those results confirm the hypothesis of degradation of organic compounds due to the formation of hydroxyl radicals, mentioned in previous studies [46]. However, as discussed above, due to the short lifetime and short diffusion of $^{\bullet}$OH radicals in bulk solution, the utilization of chemical probes, such as iodide in Weissler dosimetry, accounts for only a fraction of the radical species formed [51].

In order to verify the synergistic effects of plasma discharge and HC on the production of oxidant species, an experiment with only HC with the addition of H_2O_2 was carried out (HC + H_2O_2), as can be observed in Fig. 8. The main purpose of this experiment was to simulate the oxidant species formation rate given by sonochemical dosimetry. In experiment (HC + H_2O_2) in the absence of plasma, the only source of hydroxyl radicals was the added hydrogen peroxide. Therefore, by adding a concentration of hydrogen peroxide similar to the results of the hydroxyl radical formation would provide information about the synergistic effect between hydrodynamic cavitation and glow plasma discharge, in the formation of oxidant species.

For the HC + H_2O_2 experiment, it was possible to observe a pseudo-

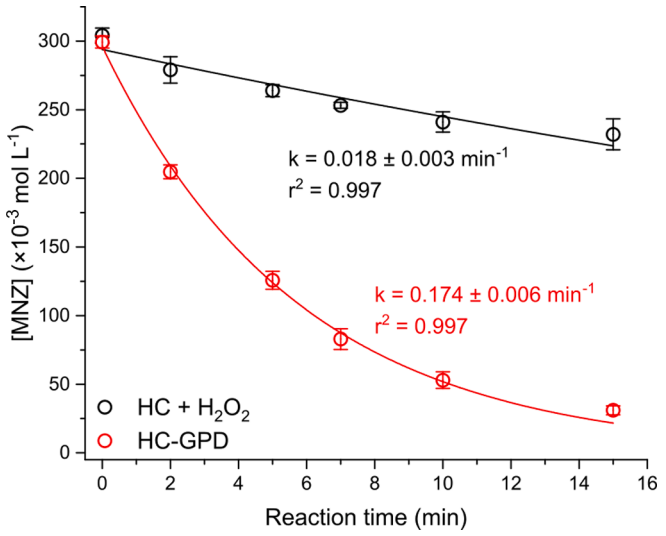

Fig. 8. Effect of H_2O_2 addition during HC process for MNZ degradation. Dots represent experimental data and continuous line the pseudo-first-order kinetic model for MNZ degradation. Experimental conditions: Experimental conditions: $[MNZ]_0 = 300 \times 10^{-3}$ mol L^{-1}, Initial pH = 5.80, Inlet pressure = 70 bar, Number of orifices = 4, Orifice size = 4 mm, Initial temperature = 14 °C, Number of replicates = 2.

first-order kinetic constant of 0.018 ± 0.003 min^{-1} for MNZ degradation, representing 23% of degradation. This constant is 9.5 times lower than the pseudo-first-order kinetic constant for MNZ degradation in HC-GPD process. Therefore, it is possible to confirm the role of the synergistic effects and •OH radicals formed in the bubble interface on the degradation of MNZ.

The utilization of electrons as a green reagent for *in-situ* formation of highly reactive •OH radicals in plasma discharge processes is an environmental-friendly approach for organic pollutants degradation [55,56,69]. *In-situ* hydrogen peroxide production prevents its dangerous handling and storage in industrial facilities. Therefore, the results as mentioned above showed the feasibility of HC-GPD system for antibiotics degradation in drinking water.

4. Conclusion

HC coupled with glow plasma discharge (HC-GPD) was proposed as a new and innovative method for the degradation of metronidazole (MNZ) in drinking water. Degradation tests provided information on the behavior of the HC-PD system for applications in drinking water. Experimental results demonstrated the feasibility of the proposed HC-GPD system in treating MNZ solutions with conductivity up to 1500 $\times 10^{-6}$ S cm^{-1}, a higher value than reported in the literature. The formation of cavitation bubbles in the HC emitter provides bubbles for the charge conduction in a glow plasma discharge. Sonochemical dosimetry provided information about the intensification of oxidant species formation under glow plasma discharge during the HC-GPD process. These results reveal potential applications for the HC-PD process to degrade organic pollutants in drinking water.

CRediT authorship contribution statement

Thiago Castanho Pereira: Methodology, Formal analysis, Writing – original draft. **Erico Marlon Moraes Flores:** Conceptualization, Writing – review & editing. **Anna V. Abramova:** Conceptualization, Writing – review & editing. **Federico Verdini:** Methodology, Formal analysis. **Emanuela Calcio Gaudino:** Conceptualization, Writing – review & editing. **Fabio Bucciol:** Methodology, Formal analysis. **Giancarlo Cravotto:** Conceptualization, Writing – review & editing.

Declaration of Competing Interest

The authors declare that they have no known competing financial interests or personal relationships that could have appeared to influence the work reported in this paper.

Acknowledgments

In memory of Prof. Vladimir Abramov, an outstanding creative scientist and a great man who knew how to combine science and friendship.

T. C. Pereira thanks to Conselho Nacional de Desenvolvimento Científico e Tecnológico (CNPq) for the doctoral scholarship (Grant No 141044/2021-7) and Fundação de Amparo à Pesquisa do Estado do Rio Grande do Sul (FAPERGS, Grant No 19/2551-0000702-7). E. M. M. Flores acknowledges Instituto Nacional de Ciência e Tecnologia de Bioanalítica (INCTBio, Process Number 88887.137487/2017-00); Conselho Nacional de Desenvolvimento Científico e Tecnológico (CNPq, Grant Nr. 313786/2019-4, 409548/2021-9, 312271/2017-4); and Fundação de Amparo à Pesquisa do Estado do Rio Grande do Sul (FAPERGS, Grant Nr. 17/2551-0000960-6, 19/2551-0000702-7, 22/2551-0000389-3, 21/2551-0002091-1); G. Cravotto thanks to the University of Turin (Ricerca Locale 2022) for the financial support.

References

[1] A.K. Thabit, K.M. Shea, O.E. Guzman, K.W. Garey, Antibiotic utilization within 18 community hospitals in the United States: A 5-year analysis, Pharmacoepidemiol. Drug Saf. 30 (2021) 403–408, https://doi.org/10.1002/pds.5156.
[2] P.F. Lanzky, B. Halting-Sørensen, The toxic effect of the antibiotic metronidazole on aquatic organisms, Chemosphere 35 (1997) 2553–2561, https://doi.org/10.1016/S0045-6535(97)00324-X.
[3] M. Wagil, J. Maszkowska, A. Białk-Bielińska, M. Caban, P. Stepnowski, J. Kumirska, Determination of metronidazole residues in water, sediment and fish tissue samples, Chemosphere 119 (2015) S28–S34, https://doi.org/10.1016/j.chemosphere.2013.12.061.
[4] S. Hena, L. Gutierrez, J.-P. Croué, Removal of metronidazole from aqueous media by C. vulgaris, J. Hazard. Mater. 384 (2020), 121400, https://doi.org/10.1016/j.jhazmat.2019.121400.
[5] Z. Fang, J. Chen, X. Qiu, X. Qiu, W. Cheng, L. Zhu, Effective removal of antibiotic metronidazole from water by nanoscale zero-valent iron particles, Desalination 268 (2011) 60–67, https://doi.org/10.1016/j.desal.2010.09.051.
[6] Y. Pan, X. Li, K. Fu, H. Deng, J. Shi, Degradation of metronidazole by UV/chlorine treatment: Efficiency, mechanism, pathways and DBPs formation, Chemosphere 224 (2019) 228–236, https://doi.org/10.1016/j.chemosphere.2019.02.081.
[7] W. Cheng, M. Yang, Y. Xie, B. Liang, Z. Fang, E.P. Tsang, Enhancement of mineralization of metronidazole by the electro-Fenton process with a Ce/SnO_2–Sb coated titanium anode, Chem. Eng. J. 220 (2013) 214–220, https://doi.org/10.1016/j.cej.2013.01.055.
[8] J.O. Ighalo, C.A. Igwegbe, A.G. Adeniyi, C.A. Adeyanju, S. Ogunniyi, Mitigation of Metronidazole (Flagyl) pollution in aqueous media by adsorption: a review, Environ Technol. Rev. 9 (2020) 137–148, https://doi.org/10.1080/21622515.2020.1849409.
[9] K. Kümmerer, A. Al-Ahmad, V. Mersch-Sundermann, Biodegradability of some antibiotics, elimination of the genotoxicity and affection of wastewater bacteria in a simple test, Chemosphere 40 (2000) 701–710, https://doi.org/10.1016/S0045-6535(99)00439-7.
[10] R. Jewell, Metronidazole, in: XPharm: The Comprehensive Pharmacology Reference, Elsevier, 2007: pp. 1–7. https://doi.org/10.1016/B978-008055232-3.62177-4.
[11] K. Kümmerer, Antibiotics in the aquatic environment – A review – Part I, Chemosphere 75 (2009) 417–434, https://doi.org/10.1016/j.chemosphere.2008.11.086.
[12] Q. Sun, G. Zhu, Enhanced Removal of Metronidazole from Aqueous Solutions via Bioelectrochemical Systems, J. Environ. Eng. 148 (2022), https://doi.org/10.1061/(ASCE)EE.1943-7870.0002006.
[13] A.C. del Álamo, M.I. Pariente, R. Molina, F. Martínez, Advanced bio-oxidation of fungal mixed cultures immobilized on rotating biological contactors for the removal of pharmaceutical micropollutants in a real hospital wastewater, J. Hazard. Mater. 425 (2022), 128002, https://doi.org/10.1016/j.jhazmat.2021.128002.
[14] M. Bahman, H. Jalili, M. Etesam, A. Amrane, Investigation of pharmaceutical compounds (Metronidazole, Rosuvastatin and Codeine phosphate) removal by Synechocystis sp. PCC6803 microalga, J. Water Process Eng. 47 (2022), 102820, https://doi.org/10.1016/j.jwpe.2022.102820.
[15] B. Wang, X. Li, Y. Wang, Degradation of metronidazole in water using dielectric barrier discharge synergistic with sodium persulfate, Sep. Purif. Technol. 303 (2022), 122173, https://doi.org/10.1016/j.seppur.2022.122173.

[16] S. Ahmadzadeh, M. Dolatabadi, Electrochemical treatment of pharmaceutical wastewater through electrosynthesis of iron hydroxides for practical removal of metronidazole, Chemosphere 212 (2018) 533–539, https://doi.org/10.1016/j.chemosphere.2018.08.107.

[17] D. Martínez-Pachón, A.M. Botero-Coy, F. Hernández, N. León López, R.A. Torres-Palma, A. Moncayo-Lasso, Elimination of contaminants of emerging concern and their environmental risk in world-real municipal wastewaters by electrochemical advanced oxidation processes, J. Environ. Chem. Eng. 10 (3) (2022) 107803.

[18] Y. Xiao, Y. Shao, M. Luo, L. Ma, D. Xu, M. Wu, G. Xu, Optimized Study and Column Experiments on Treatment Process of Metronidazole Pharmaceutical Wastewater by Microelectrolysis and Fenton Oxidation, Water Air Soil Pollut. 232 (2021) 182, https://doi.org/10.1007/s11270-021-05117-z.

[19] R. Davarnejad, Z.R. Hassanvand, S. Mansoori, J.F. Kennedy, Metronidazole elimination from wastewater through photo-Fenton process using green-synthesized alginate-based hydrogel coated bimetallic iron–copper nanocomposite beads as a reusable heterogeneous catalyst, Bioresour. Technol. Rep. 18 (2022), 101068, https://doi.org/10.1016/j.biteb.2022.101068.

[20] A. Seidmohammadi, Y. Vaziri, A. Dargahi, H.Z. Nasab, Improved degradation of metronidazole in a heterogeneous photo-Fenton oxidation system with PAC/Fe_3O_4 magnetic catalyst: biodegradability, catalyst specifications, process optimization, and degradation pathway, Biomass Convers. Biorefin. (2021), https://doi.org/10.1007/s13399-021-01668-7.

[21] Y. Li, Y. Wu, H. Jiang, H. Wang, In situ stable growth of Bi_2WO_6 on natural hematite for efficient antibiotic wastewater purification by photocatalytic activation of peroxymonosulfate, Chem. Eng. J. 446 (2022), 136704, https://doi.org/10.1016/j.cej.2022.136704.

[22] M.L. Tran, C.-C. Fu, R.-S. Juang, Removal of metronidazole by TiO_2 and ZnO photocatalysis: a comprehensive comparison of process optimization and transformation products, Environ. Sci. Pollut. Res. 25 (2018) 28285–28295, https://doi.org/10.1007/s11356-018-2848-7.

[23] T.J. Al-Musawi, N.S. Mazari Moghaddam, S.M. Rahimi, M. Amarzadeh, N. Nasseh, Efficient photocatalytic degradation of metronidazole in wastewater under simulated sunlight using surfactant- and CuS-activated zeolite nanoparticles, J. Environ. Manage. 319 (2022), 115697, https://doi.org/10.1016/j.jenvman.2022.115697.

[24] B. Mathon, M. Coquery, Z. Liu, Y. Penru, A. Guillon, M. Esperanza, C. Miège, J.-M. Choubert, Ozonation of 47 organic micropollutants in secondary treated municipal effluents: Direct and indirect kinetic reaction rates and modelling, Chemosphere 262 (2021), 127969, https://doi.org/10.1016/j.chemosphere.2020.127969.

[25] Q. Sun, G. Zhu, J. Wu, J. Lu, Z. Zhang, Simultaneous catalytic ozonation degradation of metronidazole and removal of heavy metal from aqueous solution using nano-magnesium hydroxide, Environ. Technol. 42 (2021) 894–904, https://doi.org/10.1080/09593330.2019.1648560.

[26] N. Yuan, G. Zhang, S. Guo, Z. Wan, Enhanced ultrasound-assisted degradation of methyl orange and metronidazole by rectorite-supported nanoscale zero-valent iron, Ultrason. Sonochem. 28 (2016) 62–68, https://doi.org/10.1016/j.ultsonch.2015.06.029.

[27] E.A. Serna-Galvis, A.M. Botero-Coy, D. Martínez-Pachón, A. Moncayo-Lasso, M. Ibáñez, F. Hernández, R.A. Torres-Palma, Degradation of seventeen contaminants of emerging concern in municipal wastewater effluents by sonochemical advanced oxidation processes, Water Res. 154 (2019) 349–360, https://doi.org/10.1016/j.watres.2019.01.045.

[28] H.B. Ammar, Sono-Fenton process for metronidazole degradation in aqueous solution: Effect of acoustic cavitation and peroxydisulfate anion, Ultrason. Sonochem. 33 (2016) 164–169, https://doi.org/10.1016/j.ultsonch.2016.04.035.

[29] V. Homem, L. Santos, Degradation and removal methods of antibiotics from aqueous matrices – a review, J. Environ. Manage. 92 (2011) 2304–2347, https://doi.org/10.1016/j.jenvman.2011.05.023.

[30] P. Liu, Z. Wu, A.V. Abramova, G. Cravotto, Sonochemical processes for the degradation of antibiotics in aqueous solutions: A review, Ultrason. Sonochem. 74 (2021) 105566.

[31] F.C. Moreira, R.A.R. Boaventura, E. Brillas, V.J.P. Vilar, Electrochemical advanced oxidation processes: A review on their application to synthetic and real wastewaters, Appl. Catal. B 202 (2017) 217–261, https://doi.org/10.1016/j.apcatb.2016.08.037.

[32] P.R. Gogate, A.B. Pandit, A review of imperative technologies for wastewater treatment I: oxidation technologies at ambient conditions, Adv. Environ. Res. 8 (2004) 501–551, https://doi.org/10.1016/S1093-0191(03)00032-7.

[33] S. Chandak, P.K. Ghosh, P.R. Gogate, Treatment of real pharmaceutical wastewater using different processes based on ultrasound in combination with oxidants, Process Saf. Environ. Prot. 137 (2020) 149–157, https://doi.org/10.1016/j.psep.2020.02.025.

[34] S.K. Bhangu, M. Ashokkumar, Theory of Sonochemistry, Top. Curr. Chem. 374 (2016) 56, https://doi.org/10.1007/s41061-016-0054-y.

[35] Y. Song, R. Hou, Z. Liu, J. Liu, W. Zhang, L. Zhang, Cavitation characteristics analysis of a novel rotor-radial groove hydrodynamic cavitation reactor, Ultrason. Sonochem. 86 (2022), 106028, https://doi.org/10.1016/j.ultsonch.2022.106028.

[36] E.M.M. Flores, G. Cravotto, C.A. Bizzi, D. Santos, G.D. Iop, Ultrasound-assisted biomass valorization to industrial interesting products: state-of-the-art, perspectives and challenges, Ultrason. Sonochem. 72 (2021), 105455, https://doi.org/10.1016/j.ultsonch.2020.105455.

[37] M. Ashokkumar, T.J. Mason, Sonochemistry, in: Kirk-Othmer Encyclopedia of Chemical Technology, John Wiley & Sons, Inc., Hoboken, NJ, USA, 2007. https://doi.org/10.1002/0471238961.1915141519211912.a01.pub2.

[38] D. Meroni, R. Djellabi, M. Ashokkumar, C.L. Bianchi, D.C. Boffito, Sonoprocessing: From Concepts to Large-Scale Reactors, Chem. Rev. 122 (2022) 3219–3258, https://doi.org/10.1021/acs.chemrev.1c00438.

[39] B. Wang, H. Su, B.o. Zhang, Hydrodynamic cavitation as a promising route for wastewater treatment – A review, Chem. Eng. J. 412 (2021) 128685.

[40] H. Zheng, Y. Zheng, J. Zhu, Recent Developments in Hydrodynamic Cavitation Reactors: Cavitation Mechanism, Reactor Design, and Applications, Engineering 19 (2022) 180–198.

[41] P.S. Kumar, A.B. Pandit, Modeling Hydrodynamic Cavitation, Chem. Eng. Technol. 22 (1999) 1017–1027. https://doi.org/10.1002/(SICI)1521-4125(199912)22:12<1017::AID-CEAT1017>3.0.CO;2-L.

[42] D. Crudo, V. Bosco, G. Cavaglià, G. Grillo, S. Mantegna, G. Cravotto, Biodiesel production process intensification using a rotor-stator type generator of hydrodynamic cavitation, Ultrason. Sonochem. 33 (2016) 220–225, https://doi.org/10.1016/j.ultsonch.2016.05.001.

[43] A.J. Barik, P.R. Gogate, Hybrid treatment strategies for 2,4,6-trichlorophenol degradation based on combination of hydrodynamic cavitation and AOPs, Ultrason. Sonochem. 40 (2018) 383–394, https://doi.org/10.1016/j.ultsonch.2017.07.029.

[44] V. Innocenzi, M. Prisciandaro, M. Centofanti, F. Vegliò, Comparison of performances of hydrodynamic cavitation in combined treatments based on hybrid induced advanced Fenton process for degradation of azo-dyes, J. Environ. Chem. Eng. 7 (3) (2019) 103171.

[45] V. Abramov, A. Abramova, V. Bayazitov, S. Kameneva, V. Veselova, D. Kozlov, M. Sozarukova, A. Baranchikov, I. Fedulov, R. Nikonov, G. Cravotto, Fast Degradation of Tetracycline and Ciprofloxacin in Municipal Water under Hydrodynamic Cavitation/Plasma with CeO_2 Nanocatalyst, Processes. 10 (10) (2022) 2063.

[46] V.O. Abramov, A.V. Abramova, G. Cravotto, R.V. Nikonov, I.S. Fedulov, V. K. Ivanov, Flow-mode water treatment under simultaneous hydrodynamic cavitation and plasma, Ultrason. Sonochem. 70 (2021) 105323.

[47] Y. Fang, D. Hariu, T. Yamamoto, S. Komarov, Acoustic cavitation assisted plasma for wastewater treatment: Degradation of Rhodamine B in aqueous solution, Ultrason. Sonochem. 52 (2019) 318–325, https://doi.org/10.1016/j.ultsonch.2018.12.003.

[48] R.P. Joshi, J. Qian, G. Zhao, J. Kolb, K.H. Schoenbach, E. Schamiloglu, J. Gaudet, Are microbubbles necessary for the breakdown of liquid water subjected to a submicrosecond pulse? J. Appl. Phys. 96 (2004) 5129–5139, https://doi.org/10.1063/1.1792391.

[49] C. Yamabe, F. Takeshita, T. Miichi, N. Hayashi, S. Ihara, Water treatment using discharge on the surface of a bubble in water, Plasma Processes Polym. 2 (2005) 246–251, https://doi.org/10.1002/ppap.200400077.

[50] B.R. Locke, S.M. Thagard, Analysis and review of chemical reactions and transport processes in pulsed electrical discharge plasma formed directly in liquid water, Plasma Chem. Plasma Process. 32 (2012) 875–917, https://doi.org/10.1007/s11090-012-9403-y.

[51] K.-Y. Shih, B.R. Locke, Optical and Electrical Diagnostics of the Effects of Conductivity on Liquid Phase Electrical Discharge, IEEE Trans. Plasma Sci. 39 (2011) 883–892, https://doi.org/10.1109/TPS.2010.2098052.

[52] C. Benincá, E. Charao Boni, F.F. Gonçalves, E.G. Primel, F.B. Freire, E.F. Zanoelo, Photo-fenton and UV photo degradation of naphthalene with zero- and two-valent iron in the presence of persulfate, Chem. Eng. Commun. 206 (1) (2019) 1–11.

[53] D.B. Rajamma, S. Anandan, N.S.M. Yusof, B.G. Pollet, M. Ashokkumar, Sonochemical dosimetry: A comparative study of Weissler, Fricke and terephthalic acid methods, Ultrason. Sonochem. 72 (2021) 105413.

[54] K. Fedorov, X. Sun, G. Boczkaj, Combination of hydrodynamic cavitation and SR-AOPs for simultaneous degradation of BTEX in water, Chem. Eng. J. 417 (2021), 128081, https://doi.org/10.1016/j.cej.2020.128081.

[55] B. Jiang, J. Zheng, S. Qiu, M. Wu, Q. Zhang, Z. Yan, Q. Xue, Review on electrical discharge plasma technology for wastewater remediation, Chem. Eng. J. 236 (2014) 348–368, https://doi.org/10.1016/j.cej.2013.09.090.

[56] X. Wang, M. Zhou, X. Jin, Application of glow discharge plasma for wastewater treatment, Electrochim. Acta 83 (2012) 501–512, https://doi.org/10.1016/j.electacta.2012.06.131.

[57] S. Merouani, O. Hamdaoui, F. Saoudi, M. Chiha, Sonochemical degradation of Rhodamine B in aqueous phase: Effects of additives, Chem. Eng. J. 158 (2010) 550–557, https://doi.org/10.1016/j.cej.2010.01.048.

[58] S. Talwar, A.K. Verma, V.K. Sangal, Modeling and optimization of fixed mode dual effect (photocatalysis and photo-Fenton) assisted Metronidazole degradation using ANN coupled with genetic algorithm, J. Environ. Manage. 250 (2019), 109428, https://doi.org/10.1016/j.jenvman.2019.109428.

[59] C. Wang, H. Liu, G. Wang, W. Huang, Z. Wei, H. Fang, F. Shen, Visible light driven S-scheme heterojunction $Zn_3In_2S_6$/Bi_2MoO_6 for efficient degradation of metronidazole, J. Alloy. Compd. 917 (2022), 165507, https://doi.org/10.1016/j.jallcom.2022.165507.

[60] N. Neghi, N.R. Krishnan, M. Kumar, Analysis of metronidazole removal and micro-toxicity in photolytic systems: Effects of persulfate dosage, anions and reactor operation-mode, J. Environ. Chem. Eng. 6 (2018) 754–761, https://doi.org/10.1016/j.jece.2017.12.072.

[61] H. Shemer, Y.K. Kunukcu, K.G. Linden, Degradation of the pharmaceutical Metronidazole via UV, Fenton and photo-Fenton processes, Chemosphere 63 (2006) 269–276, https://doi.org/10.1016/j.chemosphere.2005.07.029.

[62] C. Gadipelly, A. Pérez-González, G.D. Yadav, I. Ortiz, R. Ibáñez, V.K. Rathod, K. V. Marathe, Pharmaceutical Industry Wastewater: Review of the Technologies for Water Treatment and Reuse, Ind. Eng. Chem. Res. 53 (2014) 11571–11592, https://doi.org/10.1021/ie501210j.

[63] J. Rivera-Utrilla, G. Prados-Joya, M. Sánchez-Polo, M.A. Ferro-García, I. Bautista-Toledo, Removal of nitroimidazole antibiotics from aqueous solution by adsorption/bioadsorption on activated carbon, J. Hazard. Mater. 170 (2009) 298–305, https://doi.org/10.1016/j.jhazmat.2009.04.096.
[64] World Health Association, Hardness in Drinking-water, Geneva, 2010.
[65] S.G. Patra, A. Mizrahi, D. Meyerstein, The Role of Carbonate in Catalytic Oxidations, Acc. Chem. Res. 53 (2020) 2189–2200, https://doi.org/10.1021/acs.accounts.0c00344.
[66] E. Jiménez, M.K. Gilles, A.R. Ravishankara, Kinetics of the reactions of the hydroxyl radical with CH_3OH and C_2H_5OH between 235 and 360 K, J. Photochem. Photobiol. A Chem. 157 (2003) 237–245, https://doi.org/10.1016/S1010-6030(03)00073-X.
[67] F.L. Burton, G. Tchobanoglous, R. Tsuchihashi, H.D. Stensel, Metcalf & Eddy, Wastewater Engineering: Treatment and Resource Recovery, 5th ed., McGraw-Hill Education, New York, 2003.
[68] R. Pflieger, J. Lee, S.I. Nikitenko, M. Ashokkumar, Influence of He and Ar Flow Rates and NaCl Concentration on the Size Distribution of Bubbles Generated by Power Ultrasound, J. Phys. Chem. B 119 (2015) 12682–12688, https://doi.org/10.1021/acs.jpcb.5b08723.
[69] A. Asghar, A.A. Abdul Raman, W.M.A. Wan Daud, Advanced oxidation processes for in-situ production of hydrogen peroxide/hydroxyl radical for textile wastewater treatment: a review, J. Clean. Prod. 87 (2015) 826–838, https://doi.org/10.1016/j.jclepro.2014.09.010.